JOURNAL OF THERMOPHYSICS AND HEAT TRANSFER
Vol. 13, No. 4, October-December 1999

Experimental and Computational Study of High Enthalpy Double-Wedge Flows

Joseph Olejniczak,* Graham V. Candler,† and Michael J. Wright‡
University of Minnesota, Minneapolis, Minnesota 55455
and
Ivett Leyva§ and Hans G. Hornung¶
California Institute of Technology, Pasadena, California 91125

A series of experiments designed to study reacting nitrogen flow over double-wedge geometries was conducted in the T5 shock tunnel at the California Institute of Technology. These experiments were designed using computational fluid dynamics to test nonequilibrium chemistry models. Surface heat transfer rate measurements were made, and holographic Mach–Zehnder interferometry was used to visualize the flow. Analysis of the data shows that computations using standard thermochemical models cannot reproduce the experimental results. The computed separation zones are smaller than the experiments indicate. However, the computed heat transfer values match the experimental data in the separation zone, and on the second wedge the computed heat transfer distribution matches the shape and heights of the experimental distribution but is shifted due to the difference in the size of the separation zones. The most likely reasons for failure of the computations to reproduce the experimental data are uncertainties in the equilibrium and nonequilibrium nitrogen dissociation rates, non-Boltzmann vibrational energy distributions in the freestream, and possible noncontinuum effects at the model leading edge and in the shock interaction region.

Introduction

THE accurate modeling of reentry flows requires an understanding of the chemical and energy relaxation processes that occur in high-temperature gases. These thermophysical processes can alter macroscopic flow characteristics such as heating rates and shock shapes. Even subtle differences in the shock shape and the resulting differences in the pressure field can lead to large differences in the predicted aerodynamic moments of a reentry vehicle. For example, when the Space Shuttle first reentered the Earth's atmosphere, the body flap angle required to trim the orbiter was much higher than expected.[1] This pitchup anomaly was due to reacting-gas effects.

One important aspect of reacting flowfields is the coupling between the vibrational energy relaxation and the chemical dissociation process. After a gas molecule passes through a shock wave, thousands of collisions are required to raise its vibrational energy so that it is in equilibrium with the translational energy. Because of the low density and high speeds typical of reentry flows, gas molecules may travel long distances during this relaxation process, and therefore, large regions of the flowfield may be in vibrational nonequilibrium.

Molecular collisions can also cause dissociation, and the dissociation rate depends on the vibrational state of the gas. The amount of energy that a collision must supply to dissociate a molecule is the dissociation energy of the molecule minus the vibrational energy. Therefore, the dissociation rate in a region of vibrational nonequilibrium where molecules have less energy than at equilibrium is lower than in a region of thermal equilibrium. Also, because molecules with high vibrational energy are more likely to dissociate than molecules with low vibrational energy, the dissociation process slows the vibrational relaxation process by preferentially removing molecules with high vibrational energy.

Many models[2–4] exist for this vibration-dissociation coupling process, but none has been adequately validated with experimental data. Existing experimental data are not sensitive enough to vibration-dissociation coupling effects to differentiate the predictions of the coupling models. The flowfields predicted by various vibration-dissociation coupling models differ only if there is significant dissociation of molecules in regions of strong vibrational nonequilibrium. Although this nonequilibrium chemistry occurs commonly in flight, it is difficult to reproduce the necessary combination of enthalpy, density, and model size in ground-based experimental facilities.

An example of typical existing data are the measurements of shock standoff distances on spheres from the T5 Hypervelocity Shock Tunnel at the California Institute of Technology.[5] Our results, which will be presented subsequently, show that computations using any reasonable nonequilibrium rate model reproduce the data within the experimental error. The sphere experiments were not intended to provide validation data for vibration-dissociation coupling models, and the ability of current coupling models to reproduce the sphere data only shows that these blunt-body flowfields are not very sensitive to vibration-dissociation coupling effects.

Therefore, there is a need for data representative of flight conditions that is more sensitive to vibration-dissociation coupling effects. With confidence in our ability to reproduce existing experimental results from T5, we designed new experiments for T5 that can distinguish between the predictions of different coupling models.

To design these experiments, we used computational fluid dynamics to simulate the flow over many different geometries at T5 freestream conditions. Each case was computed with different coupling models. The goal was to identify the combination of geometry and freestream conditions that yields the greatest difference in the interferograms and measurable surface quantities between the two

Presented as Paper 96-2238 at the AIAA 19th Advanced Measurement and Ground Testing Technology Conference, New Orleans, LA, 17–20 June 1996; received 18 February 1999; revision received 20 July 1999; accepted for publication 20 July 1999.

*Postdoctoral Research Associate, Aerospace Engineering and Mechanics; currently Aerospace Engineer, Mail Stop 230-2, NASA Ames Research Center, Moffett Field, CA 94035. Member AIAA.

†Professor, Aerospace Engineering and Mechanics and Army High Performance Computing Research Center; candler@aem.umn.edu. Senior Member AIAA.

‡Postdoctoral Research Associate, Aerospace Engineering and Mechanics; currently Research Scientist, Eloret Institute, Moffett Field, CA 94035. Member AIAA.

§Graduate Research Assistant, Graduate Aeronautical Laboratories. Student Member AIAA.

¶Director, Graduate Aeronautical Laboratories. Member AIAA.

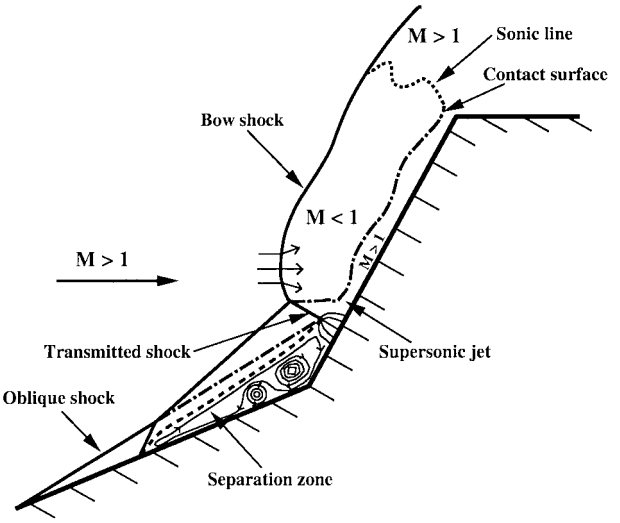

Fig. 1 Schematic diagram of the flow over a double-wedge.

computed flowfields. As a result of this design process, a double-wedge geometry was designed and tested at four angles of attack in a nitrogen freestream.

The sensitivity of the double-wedge flowfields to vibration–dissociation coupling effects is explained by considering the shock interaction that occurs near the corner of the wedges. Figure 1 shows a schematic of this flow. The shape of the detached bow shock from the second wedge depends on the nonequilibrium chemistry occurring behind it. At certain enthalpies and values of the binary scaling parameter (freestream density times a characteristic length scale) different vibration–dissociation coupling models produce slightly different bow shock shapes, resulting in different impingement points of the transmitted shock on the second wedge. Small changes in the impingement point and in this transmitted shock angle can produce large differences in the size of the separation zone because of the different amounts of mass that are reversed into the separation zone.

At relatively low wedge angles, where the separation zone size is small, there is no difference between the predictions of the vibration–dissociation coupling models. As the second wedge angle increases, the differences between the predictions of various coupling models become greater. At some large second wedge angle, the flow becomes unsteady; the predicted value of this angle depends strongly on the vibration–dissociation coupling model used.

We first discuss the results for sphere geometries, and then we present the double-wedge results. Measurements of surface heat transfer rate and interferograms were made for a range of freestream conditions and model angle of attack. Contrary to our expectations, our results show that computations with any existing flowfield model are unable to reproduce the data from the double-wedge experiments. We show evidence that the most likely reason for the discrepancies between the experimental data and the calculations is uncertainty in the nitrogen dissociation rates at both thermal equilibrium and nonequilibrium conditions. Before the acquisition of these experimental data, it was believed that the nitrogen dissociation rates at thermal equilibrium were adequately known. These results suggest otherwise, and the double-wedge experimental data provide a stringent test for proposed rate models.

Experimental Program

The experiments were performed in the T5 free-piston shock tunnel at the California Institute of Technology. Details of the facility may be found in Ref. 6 by Hornung et al. A schematic drawing of the model is shown in Fig. 2. The angle of attack of the model was varied from 0 to −17 deg (corresponding to a nose-down orientation) during the tests. The leading edge of the model was approximately 3.5 cm above the nozzle centerline and 10 cm from the nozzle exit plane during the test time. The roll angle of the model was aligned to within 0.1 mrad, and the yaw angle was aligned to within 1.0 mrad of parallel. The pitch angle, or model angle of attack, was measured to within 0.2 mrad. The T5 conical nozzle with a 7-deg half-angle and either a 20 or a 30 mm throat was used. A total of 17 runs were made, but only selected results are presented here. Table 1 lists the nominal freestream conditions at the center of the leading edge of the model for selected test cases.

Table 1 Nominal T5 freestream conditions at the leading edge of the model and model angle of attack

Shot	p_o, MPa	h_o, MJ/kg	u_∞, m/s	T_∞, K	$T_{v\infty}$, K	ρ_∞, kg/m^3	c_{N_∞}	α, deg
1035	27.5	28.5	6232	2336	4137	0.0066	0.135	−10.0
1036	26.2	28.7	6240	2311	4153	0.0063	0.140	−10.0
1038	33.2	27.3	6068	1710	3758	0.0065	0.128	−10.0
1039	32.6	28.5	6128	2887	3879	0.0145	0.152	−10.0
1043	35.1	25.7	6059	1841	3851	0.0076	0.125	−12.0
1044	33.7	23.9	5892	2163	3932	0.0090	0.080	−14.0
1046	36.5	28.1	6261	2515	4065	0.0086	0.118	−14.0
1049	36.7	26.1	6110	1888	3856	0.0078	0.129	0

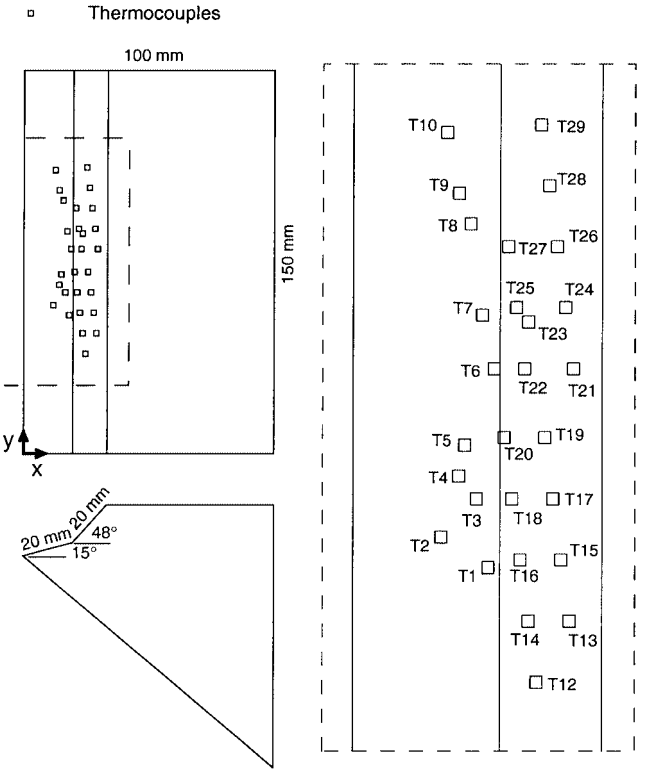

Fig. 2 Scale drawing of the double-wedge model showing.

The model was instrumented with 29 Alumel/Chromel type K thermocouples, 10 on the first wedge and 19 on the second wedge. The location of the thermocouples is shown in Fig. 2. The heat transfer rate data were sampled at a rate of 200 kHz, and the value was taken to be the average over the time window 0.8–1.2 ms. Studies of driver gas contamination in T5 show that, at the enthalpies of these tests, there is 1.0–1.2 ms of test time.[7] The heat transfer rate was deconvolved from the voltage traces using a one-dimensional semi-infinite slab model for the unsteady heat transfer to the thermocouple gauge. The details of this method are given by Sanderson and Simmons.[8]

A holographic interferometry technique developed by Sanderson[9] provided infinite fringe Mach–Zehnder interferograms, which visualize the optical path length in the flowfield relative to the optical path length in the freestream. For flowfields with constant chemical composition, visualizing optical path length is equivalent to visualizing the density field, but for these high-enthalpy flowfields, the amount of reaction affects the fringe patterns. Based on pitot

pressure measurements, the flow in the nozzle establishes in about 0.3 ms. The interferograms were taken at about 0.8 ms, which represents approximately 150 characteristic flow times based on wedge length and typical freestream conditions. Previous experimental and computational results[10,11] show that three-dimensional compression corner flows with large separation zones require only about 20 characteristic flow times to establish. Computational interferograms were generated by a straightforward line-of-sight integration through the computed three-dimensional flowfield.

Thermophysical Models

This section describes the chemical rate and energy transfer models that are needed to compute hypervelocity flowfields. Models are needed for both the vibrational equilibrium dissociation rates of nitrogen and for vibration–dissociation coupling effects. One purpose of this study is to examine the effect of model choice on the predicted flowfields.

At vibrational equilibrium, the dissociation rate for the reaction

$$N_2 + M \rightarrow N + N + M, \qquad M = N_2, N \tag{1}$$

is expressed in Arrhenius form:

$$k_f(T) = C_m\, T^{\eta_m}\, e^{-\theta_m/T} \tag{2}$$

where m is the collision partner N_2 or N and C_m, η_m, and θ_m are coefficients found from curve fits to experimentally determined data. Three different sets of coefficients from Park[12,13] and Bortner[14] were tested. The two sets of coefficients from Park are designated Park 85 and Park 88, respectively, based on the year of the reference.

Although all of the sets of coefficients were inferred from the same experimental data, the values of the rates are significantly different because of how the shock tube results were interpreted. In these experiments, nitrogen is heated by a shock wave and then undergoes dissociation. By determining the density behind the shock wave from the measured radiation signal, the dissociation rate can be deduced. However, this procedure is not straightforward. One complication is that the gas behind the shock wave does not immediately dissociate, and there is an incubation period before the onset of dissociation that is generally accepted to be caused by the vibrational relaxation process. There is no standard method to account for the vibrational nonequilibrium. For example, some investigators assume that the vibrational relaxation process ends before dissociation begins, so that the dissociation process is governed only by the translational temperature because the gas is in vibrational equilibrium. There is also difficulty in separating the dissociation rates for the two collision partners, N_2 and N. A common assumption is that the dissociation rate by N is some multiplicative factor greater than the N_2 rate. This assumption is made by Park[12,13] but not by Bortner.[14]

The Park 88 rates are different from the Park 85 because of a reinterpretation of the experimental data using the Park T–T_v vibration–dissociation coupling model to account for vibrational nonequilibrium. The Park 88 rates are perhaps the most widely accepted, and they are used for the majority of the double-wedge calculations. However, it should be emphasized that due to the difficulty in interpreting the experimental data, these reaction rates are uncertain.

Assuming that the vibrational equilibrium dissociation rates are a known function of the temperature, a vibration–dissociation coupling model is needed to account for and to determine the dependence of the vibrational nonequilibrium dissociation rate on the vibrational temperature. Any physically consistent vibration–dissociation coupling model can be written as[15]

$$k_f(T, T_v) = V(T, T_v)\, k_f(T) \tag{3}$$

where V is a coupling factor that is less than one if $T_v < T$. Three representative vibration–dissociation coupling models were tested: the Park T–T_v model,[2] the Marrone and Treanor coupled-vibration-dissociation-vibration (CVDV) model,[3] and the Macheret and Rich model.[4]

The Park T–T_v model[2] is a semi-empirical model that is widely used because it has been shown to give good results for certain test cases and because it is easy to implement. The vibrational nonequilibrium dissociation rate is assumed to be in Arrhenius form with a modified temperature:

$$k_f(T, T_v) = C_f \left(\sqrt{T\,T_v}\right)^{\eta_m} \exp\left(-\theta_m \Big/ \sqrt{T\,T_v}\right) \tag{4}$$

The CVDV model is derived by assuming that the gas may be characterized by rotationless oscillators whose vibrational energy distribution relaxes through a series of Boltzmann distributions. The model contains a preferential removal parameter U that controls how much more likely high vibrational level molecules are to dissociate than low vibrational level molecules. A value of $U = D/3$, where D is the dissociation energy of nitrogen, has been shown to give the best agreement with experimental data. In this work, we test different values of U. The Macheret and Rich model[4] is derived by generalizing the Arrhenius formula for vibrational nonequilibrium by considering a threshold energy function that determines the minimum total energy in a collision necessary for dissociation. The amount of preferential removal is fixed by the theoretically determined threshold function. The model accounts for the rotational state of the molecule and takes into account that the vibrational energy mode does not relax through a series of Boltzmann distributions. The Macheret and Rich model is theoretically the most accurate model of the three considered in this work, but it is also the most difficult to implement.

Finally, Millikan and White[16] vibration–translation relaxation rates were used in the Landau–Teller vibrational relaxation source term. The viscosity was calculated using the Blottner et al.[17] model with Wilke's[18] mixing rule, the thermal conductivity was calculated from an Eucken relation,[19] and the diffusion velocities were calculated assuming Fick's law.

Computational Method

An upwind finite-volume method given by MacCormack and Candler[20] using Steger–Warming flux vector splitting was used to solve the three-dimensional Navier–Stokes equations. Mass conservation equations for each species (N_2 and N) and a separate vibrational energy equation are solved, along with the three momentum and the total energy conservation equations. The mass and vibrational energy equations include source terms that account for the finite-rate chemistry and vibrational energy relaxation.[21] The method is second-order accurate in the streamwise and spanwise directions. The scheme is fully implicit, and uses the full matrix data parallel lower–upper relaxation (DP-LUR) method of Wright et al.[22] that was developed to efficiently solve viscous problems on massively parallel computers. The calculations were performed on a Thinking Machines CM-5 supercomputer.

It is necessary to determine the freestream conditions in T5, but this is not straightforward because there are no direct measurements of the T5 freestream. The freestream conditions must be inferred from the measured incident shock speed and pressure in the reservoir section of the nozzle. Assuming equilibrium conditions in the reservoir, the flow through the conical T5 nozzle is calculated using the Navier–Stokes solver described earlier. The computations reproduce pitot pressure measurements made in T5. Additionally, the location of the model with respect to the source of the conical flow is known, and the appropriate conically varying flow properties are used.[21]

The numerical method has been validated for separated flow calculations by matching computed surface pressure, heat transfer, and skin-friction values with experimental data[10,23] from perfect gas compression corner flows. With a sufficient number of grid points, the separation zone size and the surface quantities are matched to within experimental error. Also, comparison with perfect gas double-cone flows shows that the numerical simulations reproduce the separation zone size for flowfields with both small and large separation zones.[24,25]

The double-wedge calculations used a two-block grid of $256 \times 16 \times 256$ and $256 \times 16 \times 512$ points in the streamwise–

spanwise–body normal directions. Two-dimensional calculations show that a 256×256 grid underpredicts the separation zone size by about 4% as compared to a 512×512 grid. Grid resolution studies done in the spanwise direction show that using 16 points overpredicts the size of the separation zone at the symmetry plane by less than 6% as compared to using 24 points. Unfortunately, performing calculations on larger grids to do a true grid-resolution study is not possible with the speed and memory limits of current computers. However, grid resolution studies indicate that these calculations adequately resolve the flowfield.

Sphere Results

In this section we compare computations using various chemical rate models with previous experimental results from T5. The purpose of these comparisons is to ensure that we are able to reproduce T5 results, showing both that the calculations to characterize the T5 freestream are valid and that the thermophysical models are adequate for blunt-body hypervelocity flowfields. The flows are pure nitrogen, with the test conditions shown in Table 2. These test conditions produce flowfields with some dissociation and vibrational nonequilibrium, but these tests were not designed to be particularly sensitive to vibration–dissociation coupling effects.

Figure 3 shows the experimental and computational differential interferograms for shot 181 using the Park 85 equilibrium dissociation rates and three different vibration–dissociation coupling models. Differential interferograms measure the gradient of the optical path length using two parallel light rays slightly displaced from one another. The bow shock causes a sudden change in the shape and direction of the fringes. There are no discernible differences among the predictions of the models, and the location and shape of the experimental fringes are reproduced by all of the computational results. Shot 514 also shows no difference among the predictions of the coupling models and the experimental results.

A more quantitative comparison of the models may be made by comparing the predicted shock standoff distances, which are shown in Table 3. Both the experimental and computational standoff distances are measured from the respective interferograms. The calculations using the Park 85 equilibrium dissociation rates and any of the vibration–dissociation coupling models match the experimental standoff distances within the experimental uncertainty. The Park T–T_v coupling model[2] predicts the smallest distances, whereas the CVDV model with $U = D/8$ predicts the largest distances. Increasing the value of U in the CVDV model decreases the amount of preferential dissociation of high vibrational level molecules and decreases the shock standoff distance because more dissociation occurs from the low vibrational level molecules behind the bow shock. The standoff distances predicted by the Macheret and Rich model[4] are between the distances predicted by the Park T–T_v model[2] and the CVDV model[3] with $U = D/3$.

Table 2 T5 freestream conditions for the sphere test cases

Parameter	Shot 181	Shot 514
D, cm	10	5
u_∞, m/s	5070	4860
ρ_∞, kg/m^3	0.0402	0.0198
T_∞, K	2260	1946
$c_{N_2\infty}$	0.971	0.959
h_o	16.5	15.5

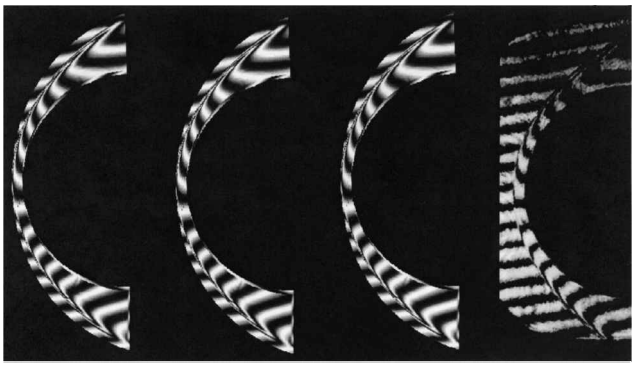

Fig. 3 Computed differential interferograms for the Park, Macheret, and CVDV models and the experimental interferogram from shot 181.

Table 3 Shock standoff distances (mm) for the sphere test case

Method	Shot 181	Shot 514
Experiment	4.83 ± 0.1	2.79 ± 0.1
Park T–T_v–Park 85	4.76	2.75
Macheret and Rich–Park 85	4.81	2.78
CVDV ($U = \infty$)–Park 85	4.77	2.79
CVDV ($U = D/3$)–Park 85	4.81	2.81
CVDV ($U = D/8$)–Park 85	4.93	2.83
Park T–T_v–Park 88	4.68	2.59
Park T–T_v–Bortner	4.59	2.49

The calculations using either the Park 85 or Bortner[14] vibrational equilibrium dissociation rates predict the smallest standoff distances, and the values fall outside the range of the listed experimental uncertainty. However, the listed experimental uncertainty only accounts for the error in measuring the standoff distances from the interferograms. The greatest difference between the prediction of any of the models and the experimental standoff distance is 11%, showing that these blunt-body flowfields are not very sensitive to the effects of chemical reactions.

In summary, existing rate models are able to reproduce the T5 sphere data. For these flow conditions, differences in the vibrational equilibrium dissociation rates have the same effect on the predicted flowfields as differences in the vibration–dissociation coupling models. Therefore, to evaluate vibration–dissociation coupling models, it is necessary to examine flowfields specifically designed to be sensitive to vibration–dissociation coupling effects.

Double-Wedge Results

In this section we present the results from the double-wedge experiments. Comparisons are made between selected shots and computations. The computations do not agree with the data, and we discuss possible reasons for this disagreement. Finally, we present additional experimental data without any comparisons to computations.

First consider shot 1049. The freestream conditions are shown in Table 1, and the Reynolds number based on the wedge face length is 1.6×10^4. The wedge angles are 18 and 48 deg, respectively, and computations predict that this flowfield is insensitive to vibration–dissociation coupling effects. Figure 4 shows the experimental and computational interferograms for this shot. The nozzle blocks the tip of the model in the experimental interferogram. Comparing the experimental interferogram with the schematic in Fig. 1, we see the same flow structure. The separation point on the first wedge cannot be seen, but the shear layer at the edge of the separation zone and the shear layer produced by the intersection of the leading-edge shock and separation shock are both visualized by dark fringes. A recirculation zone can also be seen inside the separated region. The intersection of the oblique shock with the bow shock is apparent, but because this is a relatively weak shock interaction, the transmitted shock that strikes the second wedge is difficult to see. The fan of closed fringes along the second wedge is centered just downstream of the reattachment point.

Considering the computational interferogram, we see the same basic flow structure, but the computation significantly underpredicts the size of the separation zone. The separation zone in the experiment extends over half of the first wedge, whereas in the computation, the separation zone size is only about one-fifth of the wedge face length. However, the two interferograms are qualitatively comparable. The shock impingement on the second wedge and the shape of the fringes

a) Experimental

b) Computational

Fig. 4 Interferograms for shot 1049.

look similar in both cases, but the details of these features do not match.

The number of fringes does not match either. There are approximately 11 fringes visible in the experimental interferogram, whereas there are only 9 fringes visible in the computational interferogram. Increasing the freestream density in the computations increases both the number of fringes and the size of the separation zone. However, a single, larger value of density does not simultaneously predict both the correct separation zone size and the correct number of fringes. The increase in freestream density required for a better comparison with the experimental separation zone size is about a factor of two. However, this increase in the density doubles the number of fringes in the computation, and the number of fringes is then overpredicted. This inability of the computation to reproduce the experimental flowfield is surprising. Because the numerical method has been validated for perfect gas flows with shock-induced separation regions and reacting blunt-body flowfields, we anticipated being able to compute shot 1049 accurately.

The measured surface heat transfer rate is shown in Fig. 5. The solid points represent the experimental data, and the surface has been interpolated from the points. Note that the symmetry plane of the wedge is at $y = 75.0$ mm and that the coordinate s is the distance along the wedge surface measured from the leading edge. The data show very little spanwise variation.

Figure 6 shows the comparison of the heat transfer data with the computational results on the symmetry plane. The spanwise location

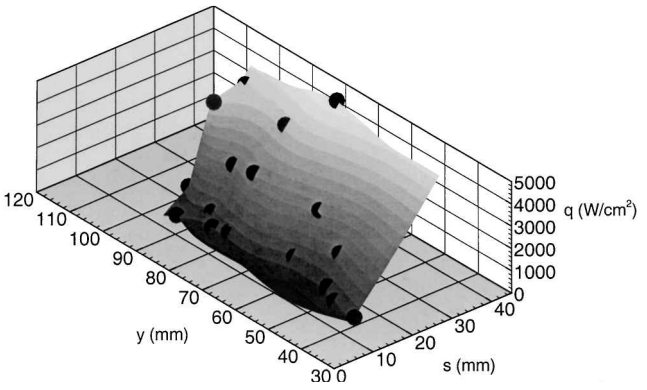

Fig. 5 Streamwise and spanwise variation of experimental heat transfer data for shot 1049.

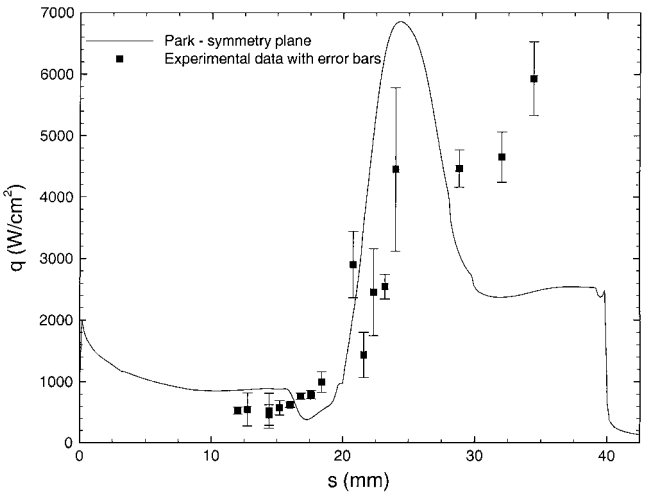

Fig. 6 Experimental heat transfer measurements for shot 1049 with computed heat transfer on symmetry plane.

of the thermocouples is ignored. The computed heat transfer rate matches the level of the experimental data in the separation zone, but the computed location of maximum heat transfer is upstream of the experimental location. This is consistent with the computation predicting a smaller separation zone than the experiment. The error bars on the data in the separation zone are fairly small, whereas in the region of the sharp rise of the heat transfer, the error bars are larger, indicating that the peak may be moving back and forth slightly. For this shot, some of the thermocouples were saturated in the region of peak heating, and those data are missing. Therefore, the true peak in the experimental heat flux is somewhat higher than the data points shown indicate.

The freestream conditions for shot 1038 (see Table 1) are similar to those of shot 1049, but the model is now at -10-deg angle of attack and the Reynolds number is 1.3×10^4. This increases the sensitivity to vibration–dissociation coupling effects because of the larger separation zone and greater sensitivity of the size of the separation zone to the location of the bow shock. The experimental and computational interferograms for shot 1038 are shown in Fig. 7. Computations were performed using both the Park T–T_v and CVDV coupling models with Park 88 vibrational equilibrium ($T_v = T$) dissociation rates. For this shot the leading edge of the model and the separation point on the first wedge are visible. Because of the slightly lower density of this shot, there is less structure visible in the separation zone, but the stronger shock interaction produces a sharply bent fringe at the location of the transmitted shock. The reattachment point on the second wedge can be inferred from the transmitted shock location. The shock-wave/boundary-layer interaction on the second wedge produces the four closed fringes visible along the second wedge. The computational interferograms are again qualitatively similar to the experimental interferogram, but the

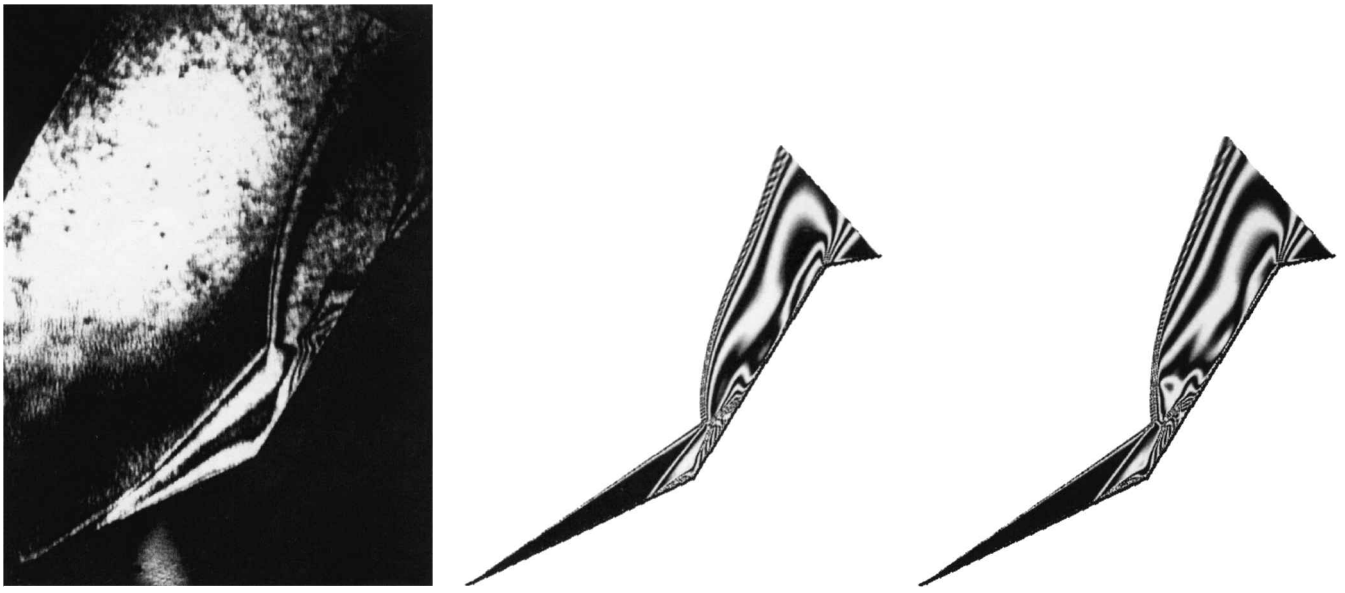

a) Experimental b) Computational with Park model c) Computational with CVDV model

Fig. 7 Interferograms for shot 1038.

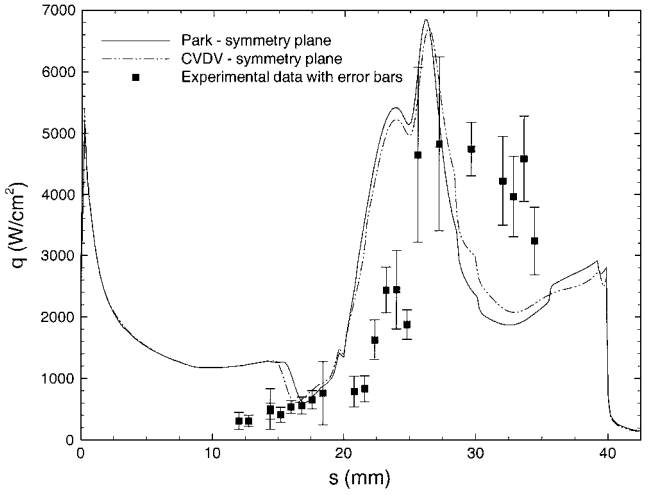

Fig. 8 Experimental heat transfer measurements for shot 1038 with computed heat transfer on symmetry plane.

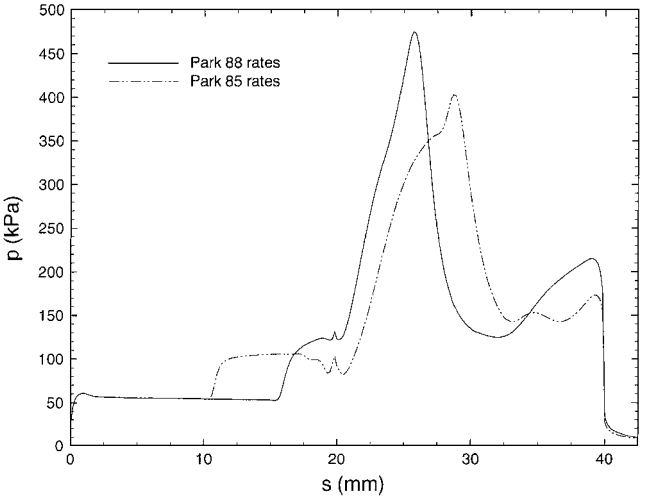

Fig. 9 Computed surface pressure on symmetry plane for two sets of equilibrium dissociation rates.

computations significantly underpredict the size of the separation zone. The CVDV model predicts a slightly larger separation zone than the Park $T-T_v$ model, but the difference between the models is small as compared to the differences of both computations with the experiment.

The heat transfer rates for shot 1038 are shown in Fig. 8. The computations appear to match the values of the experimental data in the separation region, and if the computed peaks were shifted downstream, the computation would match the data reasonably well on the second wedge. The heat transfer measurements again show little spanwise variation.

In both Figs. 7 and 8, the small differences in the size of the computed separation zones due to the choice of vibration–dissociation coupling model can be seen. Thus, the flowfield is sensitive to vibration–dissociation coupling effects; however, it is unlikely that the incorrect modeling of vibration–dissociation coupling can explain the large difference between the computed and experimental separation zones. Computations of many different combinations of double-wedge geometry and freestream conditions showed that the results of the CVDV model with $U = D/3$ and the Park $T-T_v$ model bound the sizes of the separation zones predicted by other coupling models. For example, the more realistic, and presumably more accurate, Macheret and Rich coupling predicts a separation length that falls between the predictions of the Park $T-T_v$ and the CVDV models. Presumably, for the Park 88 set of vibrational equilibrium dissociation rates, no matter which two-temperature coupling model would be used in the calculations, the computed separation zone would still be too small.

We now consider why the computations for these two shots do such a poor job of reproducing the experimental data. One possible source of error in the computations is the model of the equilibrium dissociation rates. As discussed earlier, the determination of these rates is not straightforward. Furthermore, the sphere results suggest that the Park 85 rates are slightly better at reproducing the experimental shock standoff distances. Therefore, shot 1038 was also computed using the Park 85 vibrational equilibrium dissociation rates. Figure 9 is a plot of the surface pressure along the double-wedge symmetry plane computed using the Park $T-T_v$ coupling model and the two different sets of vibrational equilibrium dissociation rates. The computation using the slower Park 85 equilibrium rates predicts a much larger separation zone than the computation using the Park 88 rates. This is a different result as compared to the sphere flowfields, where the equilibrium dissociation rates had a very small effect on the predictions. However, the size of the predicted separation zone is still significantly smaller than the experimental value. Using the CVDV coupling model with the Park 85 rates

further increases the separation zone, but it still does not match the data. The equilibrium dissociation rates would need to be even slower or the nonequilibrium rates would have to behave differently from any of the standard two-temperature vibration–dissociation coupling models predict for the computation to match the experiment.

Another possible reason for the disagreement between the computations and the experiments is turbulence in the experiments. However, this is not a factor. That the computations reproduce the measured heat transfer peak for these two cases suggests that the experimental flow is laminar. The separation zone certainly is laminar and steady, as evidenced by the small error bars on the experimental data and the ability of the computations to match these values. The large error bars for the experimental data on the second wedge show that the shock impinging on the second wedge may be moving around somewhat. However, the mean flow is established and is steady, as can be seen from the shape of the fringes from the experimental interferogram.

Both the shear layer at the edge of the separation zone and the shear layer that emerges from the triple point near the corner of the wedge are visible in the interferograms and show no sign of turbulent structures. In addition, the Reynolds number along both shear layers can be calculated from the computational data. These Reynolds numbers remain smaller than the transition Reynolds numbers reported by Birch and Keyes[26] for the transition of compressible shear layers produced by shock-on-shock interactions. The Mach number at the edge of the shear layers in the double-wedge flow falls within the Mach number range investigated experimentally by Birch and Keyes.

Finally, we show the results from additional shots. We do not present any computations of these shots because the comparisons do not yield any new information. Shot 1039 is at the same nominal conditions and angle of attack as shot 1038, except that the density is higher. Figure 10 shows the experimental interferogram. The separation zone is larger than for shot 1038, and there are more fringes because of the higher density, but otherwise the flowfields are similar. The transmitted shock is at the location where the separation shock intersects the bow shock and the fringes are strongly bent. The impingement point on the second wedge is at the center of the fan of fringes one-third of the way along the second wedge. The waviness of the fringes originating from the triple point is a possible indication that the shear layer from the triple point is turbulent. Additionally, the circular fringe along the shear layer may be caused by a vortex, indicating that the shear layer is rolling up. Because shot 1039 has the highest density of all of the shots, and the shear layer Reynolds number for this case is nearly equal to the transition Reynolds number reported by Birch and Keyes,[26] it is possible that the flowfield is turbulent downstream of the shock interaction point. However, it appears from the heat transfer data that the separation zone remains laminar. None of the interferograms from the other shots show these types of potential turbulent structures.

Fig. 10 Experimental interferogram for shot 1039.

Fig. 11 Experimental interferogram for shot 1043.

Figure 11 shows the interferogram for shot 1043. The model is at an angle of attack of −12 deg and at the same nominal conditions as shot 1049. Two-dimensional calculations predict that this flow is very sensitive to effects of vibration–dissociation coupling. Computational results also predict that shot 1043 should have a much larger separation zone than shot 1049. However, the experimental interferograms indicate that shot 1043 has only a slightly larger separation zone than shot 1049, possibly indicating that the thermochemical models used in the computations do not even predict the correct trends in the behavior of the flowfields.

Unlike shot 1039, which has a factor-of-two higher density, there are no signs of turbulent structures in the shot 1043 interferogram. The heat transfer data for shot 1043, shown in Fig. 12, has the same features as the data for the other shots: a laminar separation region followed by a sharp rise and fall in heat transfer rate.

The interferograms for shots 1035 and 1036 are shown in Figs. 13 and 14. These shots have the same nominal freestream conditions except that the density is slightly higher for shot 1035. Computations indicate the flowfields are sensitive to vibration–dissociation coupling effects. The interferograms are very similar. The separation zone for shot 1035 is slightly larger because of the larger density. The flowfields below the leading edge are different because for shot 1035 pressure transducers were installed on the first wedge and the casings for them alter the bottom surface of the model.

The interferograms for shots 1044 and 1046 are shown in Figs. 15 and 16. The model is at an angle of attack of −14 deg, and because of this, the flowfield is very sensitive to vibration–dissociation coupling effects. The flowfield is also more three-dimensional than the earlier flowfields because of the larger separation zone. The dark fringes originating on the first wedge are thought to show the extent of the separation region at various spanwise locations. Thus, the difference between the separation length at the wedge symmetry plane and at the edges is considerable.

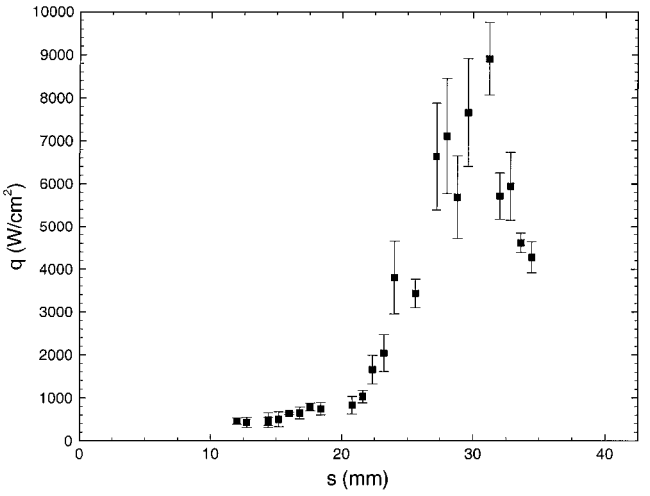

Fig. 12 Experimental heat transfer measurements for shot 1043.

Fig. 13 Experimental interferogram for shot 1035.

Correspondingly, the location of the transmitted shock that strikes the second wedge varies in the spanwise direction. Shot 1046 has a higher enthalpy and slightly lower density than shot 1044, resulting in separation zone sizes that are approximately the same.

Based on these results and other results that have not been presented, we can make some general comments. The experimental data are believed to be valid. The heat transfer rate data are consistent with the computational results. The numerical method has been validated for perfect gas compression corner flows and double-cone flows, so that it is thought the computations should be able to reproduce the experimental data. Of the models used in the computations, the thermochemical models, such as the expression for the equilibrium and nonequilibrium dissociation rates, have the most uncertainty. Before this work was performed, it was believed that the current models were adequate for most hypersonic flows and that this work would seek to distinguish subtle differences between the various chemistry models that would become apparent in only very specific flowfields. The double-wedge data suggest that the accuracy of the current models is much worse than previously believed. One possibility is that the values of the equilibrium dissociation

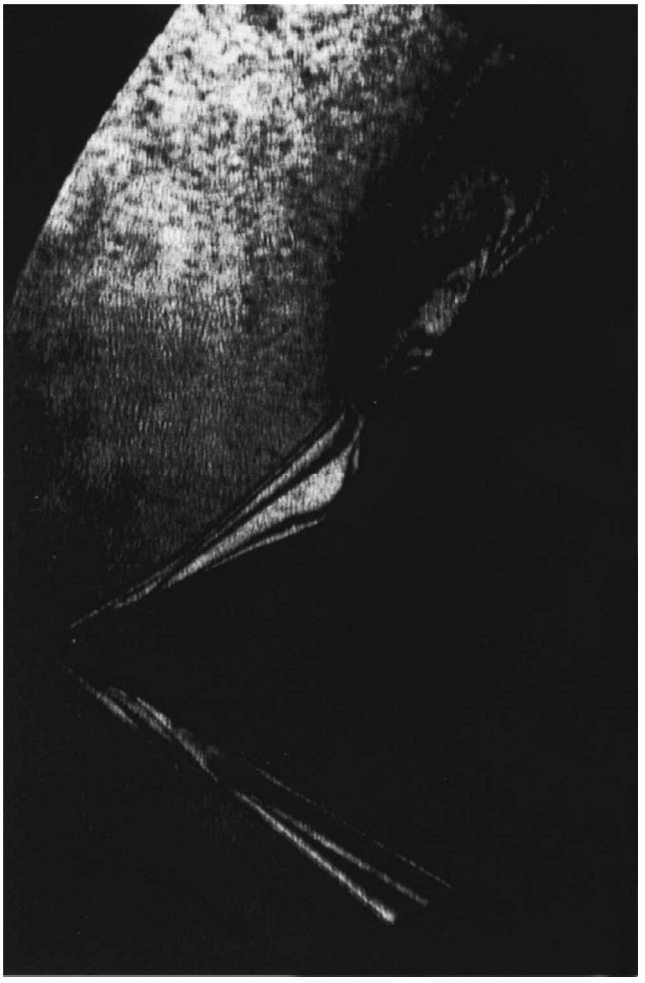

Fig. 14 Experimental interferogram for shot 1036.

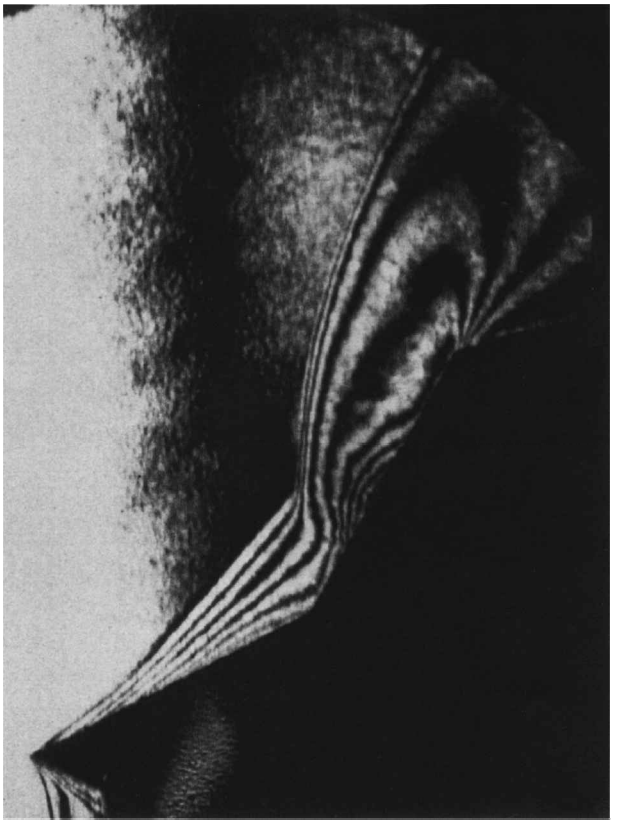

Fig. 15 Experimental interferogram for shot 1044.

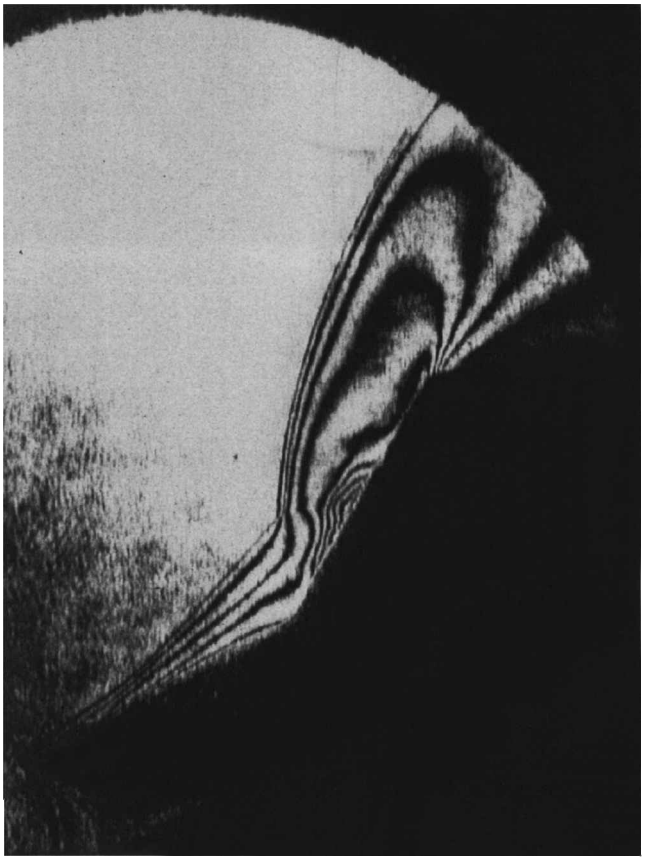

Fig. 16 Experimental interferogram for shot 1046.

rates are not as well known as previously believed. For example, if these rates were slower, the computed separation zone sizes would be larger. Related to this possible problem with the rates is the effect of non-Boltzmann vibrational energy distributions in the tunnel freestream on the effective reaction rates. It is well known that these suddenly expanded flows have elevated levels of vibrationally excited molecules. Thus, on average the gas tends to dissociate more easily than a gas at the assumed Boltzmann vibrational energy distribution. To assess the importance of this effect, it would be necessary to perform a vibrational state-specific simulation of these flows. This is beyond any existing capability.

Another possible source of discrepancy between the computations and experiments is due to noncontinuum effects in the flowfield. By most conventional measures, these flows are continuum, with a maximum Knudsen number based on freestream conditions and the wedge face length of 7.8×10^{-4} (shot 1036). However, at the wedge leading edge and in the shock interaction region, the continuum formulation may fail. In both cases, the continuum approach may impose an artificially small length scale on the flow, resulting in overly strong leading edge and shock interactions. Again, it is beyond current computational capabilities to determine if this effect causes the lack of agreement between the computations and experiments.

Conclusions

High-enthalpy tests of double-wedge geometries have been conducted in the T5 shock tunnel. Data from a range of freestream conditions and model angles of attack have been obtained. The experimental flows were laminar, and there was sufficient test time to produce steady flows. The purpose of these experiments was to obtain data to test vibration–dissociation coupling models used in hypersonic flow calculations. However, computations using a state-of-the-art vibrational nonequilibrium finite-rate nitrogen dissociation flowfield model are unable to reproduce the experimental data, even for conditions that show little dependence on vibration–dissociation coupling effects. The computations significantly underpredict the size of the separation zones. However, the computations reproduce the heat transfer rate data in the separation region and match the height and shape, but not the location of the heat transfer peak on the second wedge. For conditions that are sensitive to vibration–dissociation coupling, the CVDV model matches the data slightly better than the Park T–T_v model, but neither coupling model predicts the correct trends in the data as a function of model angle of attack or freestream density.

Grid convergence studies show that the calculations are grid resolved, and the thermochemical models used are the best available. The most likely reasons for the disagreement between the computations and experiments are uncertainties in the equilibrium and nonequilibrium dissociation rates, the presence of a non-Boltzmann vibrational energy distribution in the tunnel freestream, and the failure of the continuum formulation in the strong interaction regions.

Acknowledgments

This work was supported by Air Force Office of Scientific Research Grant F49620-93-1-0338 and NASA Langley Research Center Grant NAG-1-1498. This work is also sponsored in part by the Army High Performance Computing Research Center under the auspices of the Department of the Army, Army Research Laboratory Cooperative Agreement DAAH04-95-2-0003/Contract DAAH04-95-C-0008. The experimental results could have not have been obtained without the help of Bahram Valiferdowski, Jean-Paul Davis, Patrick Lemieux, and Phillipe Adam at the Graduate Aeronautical Laboratories, California Institute of Technology. We are especially grateful to Simon Sanderson, whose help was essential in using the holographic interferometer.

References

[1]Maus, J. R., Griffith, B. J., and Szema, K. Y., "Hypersonic Mach Number and Real Gas Effects on Space Shuttle Orbiter Aerodynamics," *Journal of Spacecraft and Rockets,* Vol. 21, 1984, pp. 126–141.

[2]Park, C., "Assessment of Two-Temperature Kinetic Model for Dissociating and Weakly Ionizing Nitrogen," AIAA Paper 86-1347, June 1986.

[3]Marrone, P. V., and Treanor, C. E., "Chemical Relaxation with Preferential Dissociation from Excited Vibrational Levels," *Physics of Fluids*, Vol. 6, No. 9, 1963, pp. 1215–1221.

[4]Macheret, S. O., and Rich, J. W., "Theory of Nonequilibrium Dissociation Rates Behind Strong Shock Waves," AIAA Paper 93-2860, July 1993.

[5]Wen, C., "Hypervelocity Flow over Spheres," Ph.D. Dissertation, Graduate Aeronautical Labs., California Inst. of Technology, Pasadena, CA, Feb. 1994.

[6]Hornung, H. G., Sturtevant, B., Belanger, J., Sanderson, S. R., Brouillette, M., and Jenkins, M., "Performance Data of the New Free-Piston Shock Tunnel T5 and GALCIT," *Proceedings of the 18th ISSW Conference*, 1991.

[7]Sudani, N., and Hornung, H. G., "Detection of Driver Gas Contamination in the T5 Hypervelocity Shock Tunnel," AIAA Paper 97-0561, Jan. 1997.

[8]Sanderson, S. R., and Simmons, J. M., "Drag Balance for Hypervelocity Impulse Facilities," *AIAA Journal*, Vol. 29, No. 12, 1991, pp. 2185–2197.

[9]Sanderson, S. R., "Shock Wave Interaction in Hypervelocity Flow," Ph.D. Dissertation, Graduate Aeronautical Labs., California Inst. of Technology, Pasadena, CA, May 1995.

[10]Holden, M. S., and Moselle, J. R., "Theoretical and Experimental Studies of the Shock Wave–Boundary Layer Interaction on Compression Surfaces in Hypersonic Flow," Aerospace Research Lab., TR ARL 70-0002, Wright–Patterson AFB, OH, Jan. 1970.

[11]Rudy, D. H., Thomas, A. K., Gnoffo, P. A., and Chakravarthy, S. R., "Laminar Hypersonic Compression-Corner Flows," *AIAA Journal,* Vol. 29, No. 7, 1991, pp. 1108–1113.

[12]Park, C., "On Convergence of Computation of Chemically Reacting Flows," AIAA Paper 85-0247, Jan. 1985.

[13]Park, C., "Two-Temperature Interpretation of Dissociation Rate Data for N_2 and O_2," AIAA Paper 88-0548, Jan. 1988.

[14]Bortner, M. H., "A Review of Rate Constants of Selected Reactions of Selected Reactions of Interest in Re-Entry Flow Fields in Atmosphere," NBS TN 484, 1969.

[15]Olejniczak, J., and Candler, G. V., "Vibrational Energy Conservation with Vibration–Dissociation Coupling: General Theory and Numerical Studies," *Physics of Fluids,* Vol. 7, No. 7, 1995, pp. 1764–1774.

[16]Millikan, R. C., and White, D. R., "Systematics of Vibrational Relaxation," *Journal of Chemical Physics*, Vol. 39, No. 12, 1963, pp. 3209–3213.

[17]Blottner, F. G., Johnson, M., and Ellis, M., "Chemically Reacting Viscous Flow Program for Multi-Component Gas Mixtures," Sandia National Lab., Rept. SC-RR-70-754, Albuquerque, NM, 1971.

[18] Wilke, C. R., "A Viscosity Equation for Gas Mixtures," *Journal of Chemical Physics*, Vol. 18, No. 4, 1950, pp. 517–519.

[19] Vincenti, W. G., and Kruger, C. H., *Introduction to Physical Gas Dynamics*, Krieger, New York, 1975, pp. 15–23.

[20] MacCormack, R. W., and Candler, G. V., "The Computation of Hypersonic Ionized Flows in Chemical and Thermal Nonequilibrium," *Computers and Fluids*, Vol. 17, No. 1, 1989, pp. 135–147.

[21] Olejniczak, J., "Computational and Experimental Study of Nonequilibrium Chemistry in Hypersonic Flows," Ph.D. Dissertation, Dept. of Aerospace Engineering and Mechanics, Univ. of Minnesota, Minneapolis, MN, April 1997.

[22] Wright, M. J., Candler, G. V., and Prampolini, M., "A Data-Parallel LU Relaxation Method for the Navier–Stokes Equations," *AIAA Journal,* Vol. 34, No. 7, 1996, pp. 1371–1377.

[23] Sinha, K., Wright, M. J., and Candler, G. V., "The Effect of Turbulence on Double-Cone Shock Interactions," AIAA Paper 99-0146, Jan. 1999.

[24] Wright, M. J., Olejniczak, J., Candler, G. V., Magruder, T. D., and Smits, A. J., "Numerical and Experimental Investigation of Double-Cone Shock Interactions," AIAA Paper 97-0063, Jan. 1997.

[25] Wright, M. J., "A Family of Data-Parallel Relaxation Methods for the Navier–Stokes Equations," Ph.D. Dissertation, Dept. of Aerospace Engineering and Mechanics, Univ. of Minnesota, Minneapolis, MN, June 1997.

[26] Birch, S. F., and Keyes, J. W., "Transition in Compressible Free Shear Layers," *Journal of Spacecraft and Rockets*, Vol. 9, No. 8, 1972, pp. 623–624.